Effect of Aging Time and Film Thickness on the Photoelectrochemical Properties of TiO2 Sol-Gel Photoanodes

Journal Article

Author(s):
Regonini, Domenico; Alves, Annelise K.; Berutti, Felipe A.; Clemens, Frank Jörg (iD)

Research Article

Effect of Aging Time and Film Thickness on the Photoelectrochemical Properties of TiO$_2$ Sol-Gel Photoanodes

D. Regonini,[1] A. K. Alves,[2] F. A. Berutti,[2] and F. Clemens[1]

[1] *Laboratory for High Performance Ceramics, Swiss Federal Laboratories for Materials Science and Technology (EMPA),*
 Überlandstrasse 129, 8600 Dübendorf, Switzerland
[2] *Laboratory of Ceramic Materials, Federal University of Rio Grande do Sul, 99 Osvaldo Aranha Avenue,*
 90035-190 Porto Alegre, RS, Brazil

Correspondence should be addressed to D. Regonini; domenico.regonini@empa.ch and F. Clemens; frank.clemens@empa.ch

Received 10 April 2014; Accepted 21 July 2014; Published 25 August 2014

Academic Editor: Jiaguo Yu

This work has focused on the investigation of a non-aqueous based sol-gel process to produce TiO$_2$ based photoelectrodes for solar water splitting. In particular, the effect of the aging time of the sol and TiO$_2$ film thickness on the photoelectrochemical properties of the photoanodes has been investigated. In order to achieve optimal performances (i.e., photocurrent density up to 570 μA/cm^2 and IPCE of 26% at 300 nm), the sol needs to be aged for 3 to 6 h, before being dip-coated to produce the photoanodes. The importance of the aging time can also be appreciated from the optical properties of the TiO$_2$ films; the absorbance threshold of the sol-gel aged for 3–6 h is slightly shifted towards longer wavelenghts in comparison to 0 h aging. Aging is necessary to build up a well-interconnected sol-gel network which finally leads to a photoelectrode with optimized light absorption and electron collection properties. This is also confirmed by the higher IPCE signal of aged photoelectrodes, especially below 340 nm. Among thicknesses considered, there is no apparent significant difference in the photoresponse (photocurrent density and IPCE) of the TiO$_2$ sol-gel films.

1. Introduction

The photoelectrochemical solar water splitting promoted by TiO$_2$ has been first reported in 1972 by Fujishima and Honda [1] and extensively investigated over the last 40 years [2–4]. TiO$_2$ is recognized as an environmentally friendly, economically accessible, photostable, and biologically inert photocatalyst [3, 4], although its large band-gap (3.0 to 3.2 eV) allows only the absorption of a small portion of the photons available from the solar spectrum [3]. To date, various attempts to modify the band-gap of TiO$_2$ by introducing suitable dopants within its lattice [3, 5, 6] have failed to deliver a material with an enhanced photoactivity. Such doping increases visible light absorption but increases also the probability of charge carriers recombination (i.e., new defects formed within the doped structure act as traps [7] for e$^-$ and h$^+$). More promising results are instead obtained by inducing oxygen nonstoichiometry in TiO$_2$ via thermal treatment in a reducing atmosphere; in this case, the conductivity and to some extent the optical properties of the oxide are improved and the photoactivity is also enhanced, with the oxide remaining free from defects typically introduced whenever attempting to dope with foreign species [8–10]. It is also possible to optimize the electron transport properties of TiO$_2$ by selecting the most appropriate morphology for a given application [11, 12]. Concerning solar driven water splitting, Hartmann et al. [13] suggested that mesoporous TiO$_2$ sol-gel represents the ideal morphology to ensure good electronic interconnectivity and therefore a much more efficient collection of the photogenerated e$^-$ than in TiO$_2$ nanoparticles. It should also be considered that, unlike mesoporous sol-gel films, TiO$_2$ nanoparticles are too small to support an inbuilt electrical field [14], meaning there is no space-charged layer [15] to assist the water splitting process. Under such conditions, the surface intermediates (Ti$_s$–O$^\bullet$ radicals, Ti$_s$–O–O–Ti$_s$ peroxo species) involved in the photooxidation of water act as scavengers of e$^-$ in the conduction band of TiO$_2$ nanoparticles; hence, the photocurrent is drastically

reduced [11]. Concerning the electron transport within a network of nanoparticles, it has been shown that it is aided by self-doping, occurring under illumination and enhancing the conductivity of the nanoparticles [16]. Therefore, Augustyński et al. [15] argue that the superior water splitting performances of sol-gel should not be ascribed to the good electronic interconnectivity but rather to the absence of a space-charged layer in the case of nanoparticles. Based on our recent studies on TiO_2 sol-gel, electrospun fibres, and nanoparticles [17], we suggest that both the absence of an inbuilt electric field in nanoparticles and the better interconnectivity (due to the Ti–O–Ti network) within the sol-gel are contributing to the better performances of sol-gel photoanodes. Among the possible sol-gel routes to obtain TiO_2 from a Ti alkoxide precursor, a better control over the structure of the sol and nanocrystallinity in the spin- (or dip-) coated films can be established, for example, by replacing water with an organic acid and an alcohol and also by using nonionic surfactants such as Triton X-100 [18] or Tween 20 [19, 20]. A similar approach is adopted and implemented within this work. As discussed later in Section 3, an added value and novelty of this work are the development of a system where the thickness of the film is not influenced by the aging time and the viscosity of the sol but only by the number of dip-coated layers. This allows a direct comparison between photoanodes aged for different times (as they have the same thickness). Furthermore, only few studies on the effect of film thickness on the photochemistry of the sol-gel are available to date. Yasumori et al. [21, 22] showed a nearly linear correlation between the thickness (up to 400 nm) of sol-gel photocatalyst and the amount of H_2 produced. Similarly, it has been recently reported that at a given wavelength (365 nm) the IPCE also increases (almost) linearly with the thickness of TiO_2 sol-gel photoanode (maximum thickness investigated was 1.3 μm) [23]. Nevertheless, further investigations are required to understand to which extent (in terms of thickness, porosity, aging, and crystallinity) a carefully chosen sol-gel synthetic route can lead to TiO_2 photoanodes with optimal electron transport properties. The aims of this work are

(i) to investigate the effect of film thickness on the photocurrent density and the IPCE response of TiO_2 sol-gel films,

(ii) to optimize the photoelectrochemical properties of our sol-gel processing method [17, 24] by investigating the influence of aging time on the performances of TiO_2 photoanodes.

As a result of this study, a robust correlation between the processing method (aging and thickness), the microstructure, and crystallinity of the sol-gel photoelectrodes and their photoelectrochemical properties is established by the use of different characterization techniques (Section 2.2) and presented in detail in Section 3.

2. Materials and Methods

2.1. Fabrication of TiO_2 Sol-Gel Photoelectrodes.

The sol-gel photoelectrodes were prepared according to the following procedure: 2.84 mL (9.6 mmol) of titanium tetraisopropoxide [$Ti(OPr^i)_4$, Merck] was mixed in 2.84 mL (50 mmol) of acetic acid (Sigma-Aldrich) and kept under magnetic stirring for 10 minutes. The sol was then additionally kept in the dark for 15 minutes, before adding 0.8 mL (7.8 mmol) of acetylacetone (Acac, Sigma-Aldrich), 0.1 mL of Triton-x-100 (Sigma-Aldrich) [24], and a solution of 0.32 g (5wt.%) of PVB (Mowital B 30H, Omya) in 8 ml of dry EtOH. The sol was finally aged in the dark for different times, 0 h (i.e., no aging), 3 h, or 6 h, before being dip-coated (Compact DipMaster 50 Dip Coater, Chemat Scientific Inc.) on FTO glass substrates (Pilkington NSG TEC 8A, Xop Física) previously cleaned by sonication in isopropanol for 10 minutes, rinsed with distilled water and EtOH, and dried under an air flow. Dip coating parameters to obtain a 1-layer-thick green sol-gel photoelectrode were (a) substrate dipping/withdrawal speed of 50 mm/min and (b) dipping time of 30 s. In the case of multilayered films, the entire procedure described above was repeated to obtain 2 or 3 layers of green sol-gel photoanodes. All the photoelectrodes were left to dry for 24 h before being calcinated at 500°C in air (heating rate of 1.6°C/min, dwelling time: 2 h). In the case of multilayers photoanodes, the time interval between each dip coating was also kept for 24 h and the calcination done only once, when all the desired layers had been dip-coated on the FTO glass.

2.2. Characterization

2.2.1. Rheology.
Measurements were performed using a Rheolab MC 120 (Anton Paar GmbH, Germany) rheometer. The viscosity (Pa·s) and the shear stress (Pa) of the sols were measured as a function of the shear rate (from 100 to 1000 s^{-1}) at different time intervals (0, 3, and 6 h) to monitor changes of flow behavior occurring during the aging process.

2.2.2. Morphology, Microstructure, and Crystallinity.
The morphology, microstructure, and thickness of the photoelectrodes were analyzed by scanning electron microscopy (SEM, either TS5136 MM-Tescan or a Field Emission Nova NanoSEM 230-Nova FEI) and the crystal phases determined by grazing angle X-ray diffraction (GAXRD) analysis, performed on TiO_2 thin film photoelectrodes (grazing angle ω = 1°, using a Panalytical, X'Pert Pro instrument (Cu-Kα1, λ = 1.5406 Å). The porosity of the thin film photoelectrodes was estimated from SEM images using the freeware ImageJ.

2.2.3. Specific Surface Area of Photoelectrodes.
The surface area of the thin films was determined by dye adsorption/desorption measurements, using a commercial N719 dye (Sigma-Aldrich), assuming a dye monolayer coverage of the TiO_2 and a dye molecular footprint of 180 $Å^2$ [26]. Photoelectrodes were first left to dry at 80°C overnight and then soaked for 3 h in a 0.2 mM solution of N719 in tert-butanol/acetonitrile (1:1 in volume). Samples were removed

from the above solution, rinsed with EtOH and acetonitrile, and left to dry at 60°C for 1 h. The N719 dye adsorbed onto the TiO$_2$ films was desorbed by soaking (1 h) the films in a known volume of 0.01 M KOH in water. From UV-Vis (UV 3600 Spectrophotometer, Shimadzu) absorbance analysis and knowing the porosity of the films, it was then possible to calculate the specific surface area of the TiO$_2$ photoelectrodes aged for different times.

2.2.4. Photoelectrochemical and Optical Characterizations. The photocurrent measurements were performed using a 3-electrode system (working electrode: TiO$_2$ photoanode; counter electrode: platinum plate, XM120, Radiometer Analytical; reference electrode: Ag/AgCl/3M-KCl, XR300, Radiometer Analytical) inserted into a cappuccino cell [27] filled with 10 mL of 1 M KOH solution (pH = 13.8) and connected to a potentiostat (Voltalab80 PGZ 402, Radiometer Analytical). The cappuccino cell was irradiated by a Xe lamp (solar simulator, Oriel Lamp by LOT-Oriel AG), at an intensity correspondent to 1.5AM (1 sun, 1,000 W/m^2), and the resulting photocurrent density (J) measured as a function of a potential sweep from −900 to +600 mV (vs the Ag/AgCl ref. electrode), at a scan rate of 20 mV/sec.

Additionally, incident photon to current efficiency (IPCE) action spectra were also performed adopting a 2-electrode system, using a Xe lamp (by LOT-Oriel AG) as light source and a monochromator (Omni-λ 300, LOT-Oriel AG). A typical experiment consisted in illuminating a TiO$_2$ photoanode (immersed in 1 M KOH) with light of wavelength (λ) ranging from 600 nm to 300 nm (at 1 nm step). A Keithley 2450 source meter was used to provide a bias (0.00 V or 0.23 V) between the photoanode and a Pt counter electrode and to measure the photocurrent as a function of the wavelength, $J_{\text{Photo}}(\lambda)$. The power of the irradiating source, $P(\lambda)$, was recorded with a ThorLabs PM100USB power meter and the IPCE(λ)% values calculated as

$$\text{IPCE}(\lambda)\% = 1240 \cdot \left(\frac{J_{\text{Photo}}(\lambda) \ \left(\mu\text{A} \cdot \text{cm}^{-2} \right)}{\lambda \cdot P(\lambda) \ \left(\text{nm} \cdot \text{W} \cdot \text{m}^{-2} \right)} \right). \quad (1)$$

For the photocurrent and IPCE measurements, a minimum of 5 specimens for each different type of photoelectrodes were tested and results are given together with their relative standard deviations. UV-Visible analysis (UV 3600 Spectrophotometer, Shimadzu) was performed to determine the transmittance and diffuse reflectance of the photoelectrodes (T_{TiO_2}, R_{TiO_2}) and the FTO substrate (T_{FTO}, R_{FTO}), ranging λ from 650 to 250 nm (sampling interval 1 nm). The absorbance, that is, optical density, opt. dens. (λ), is then given by

$$\text{Opt. dens. } (\lambda) = -\text{Log}_{10} \left(\frac{\left(T_{\text{TiO}_2}/T_{\text{FTO}} \right)}{1 - \left(\left(R_{\text{TiO}_2} - R_{\text{FTO}} \right)/100 \right)} \right)$$
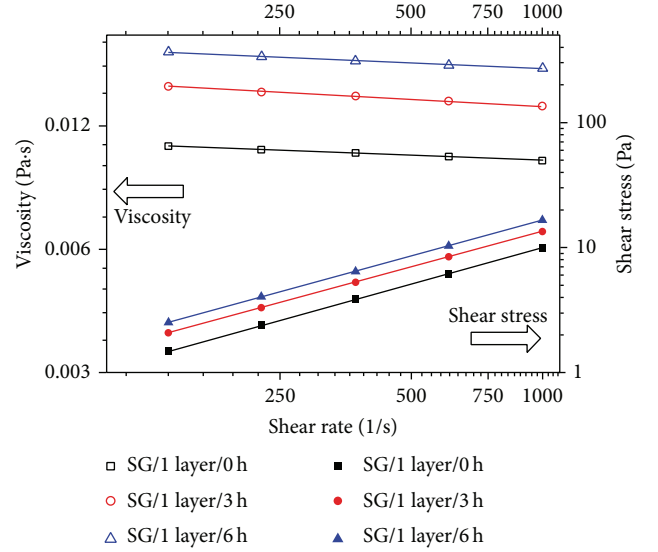$$= \frac{\alpha \cdot d}{2.303}, \quad (2)$$

Figure 1: Rheology measurements showing how the viscosity and shear stress of the sol change during the aging process.

Table 1: Thickness of sol-gel TiO$_2$ photoelectrodes measured by SEM. The indirect band-gap obtained from the Tauc plot [25] applied to the optical data in Figure 3 is also given.

Photoelectrode	Thickness (d) (μm)	Indirect band-gap (eV)
0 h aging, 1 layer	0.6 ± 0.1	3.25 ± 0.08
3 h aging, 1 layer	0.6 ± 0.1	3.25 ± 0.06
6 h aging, 1 layer	0.6 ± 0.1	3.21 ± 0.08
6 h aging, 2 layers	1.1 ± 0.1	3.22 ± 0.06
6 h aging, 3 layers	1.6 ± 0.2	3.21 ± 0.02

where α is the absorption coefficient and d is the thickness of the film. The indirect band-gap of the photoelectrodes was extrapolated from a plot of $(\alpha h\nu)^{1/2}$ versus $h\nu$, Tauc plot [25].

3. Results and Discussion

As expected, the rheology measurements performed on the TiO$_2$ sol-gel system, Figure 1, are showing an increase in shear stress and viscosity occuring during the aging process of the sol, which was monitored at 0, 3, and 6 h. The increase in shear stress and viscosity is more pronounced between 0 and 3 h than between 3 and 6 h aging, suggesting that the most significant physical and chemical changes within the TiO$_2$ sol are occuring within the first 3 h of the aging process. This is in good agreement with previous reports on the preparation of sols using metal alkoxide based precursors [28]. The results of the SEM analysis, summarized in Table 1, reveal that aging time has no effect on the thickness of the photoanode, which remains as 0.6 ± 0.1 μm for 1 layer TiO$_2$ dip-coated after 0, 3, or 6 h aging. This was expected, considering there is no real gelling effect (i.e., shear thinning effect) in the TiO$_2$ sol; from Figure 1, it is clear that the sol behaves almost as a new-tonian fluid [29]. The viscosity is almost independent of the shear rate and the shear stress shows linear behavior versus

the shear rate. It is therefore assumed that the film thickness is mainly influenced by the solid TiO_2 content (kept constant in this study) inside the sol-gel system. The TiO_2 sol system does not show a real gelling effect for the following reasons.

(i) The water required for hydrolysis of $Ti(OPr^i)_4$ is initally absent and it is only slowly released in the sol via reaction between the alcohol (EtOH) and the acetic acid. The Ti–O–Ti network can also be created by alcoholysis of the Ti alkoxide precursor, which again is slower than hydrolysis and easier to control [18].

(ii) It has been previously shown that chelating agent such as Acac, used in this study, despite causing the Ti alkoxide precuorsor to be more prone to hydrolysis/alcoholysis, is in fact slowing down (or preventing) gelation because it offers alternative paths to the polymerization reaction [30].

(iii) An excess of acetic acid is used in our system and this is also known to retard the gelation of Ti alkoxides by promoting the formation of stabilized dimeric complexes (the coordination of Ti also changes from 4 to 6 upon addition of acetic acid) [29].

Our study shows that it is possible to prepare films with thickness independent of aging time; as previously mentioned, this allows evaluating the impact of aging time on the ability of the photoelectrodes to sustain electron transport.

The results of the GAXRD analysis of the photoelectrodes (after calcination at 500°C) are summarized in Figure 2. Anatase is the dominant phase (>95%) in all the photoelectrodes, although a small amount of rutile is also present. An additional and important fact emerging from Figure 2 is the impact of the sol-gel aging process on the crystallinity of the film. By comparing the XRD spectra of 1-layer-thick photoelectrodes (i.e., same thickness) without aging (0 h) and aged for 3 or 6 h, the anatase peaks appear to be more pronounced in the case of aged films. In other terms, when the aging step is not performed (0 h), the XRD signals of the FTO substrates dominate over the TiO_2 peaks. This is best appreciated when comparing the anatase peak at 25.4° and the FTO peak at 26.6°. Crystallinity is indeed a very important requirement towards the design of effective photocatalysts for the formation of H_2 via solar water splitting [31]. Additionally, the analysis of the crystalline particles size by applying the Scherrer equation [32] to the anatase peak (101) at $2\theta = 25.3 - 25.4°$, Figure 2, reveals that they are sufficiently big to allow efficient electron transport. The size of the crystalline domains for all the different photoelectrodes is approximately 30 nm and sufficiently larger domains (at least >15 nm) are generally suggested to be required to facilitate transport of electrons during the water splitting process [13].

Despite having no significant effect on the thickness of TiO_2 films, aging time appears to influence the optical properties of the photoanodes, as shown in Figure 3; the absorbance threshold of the sol-gel aged for 3 and 6 h is slightly shifted towards higher wavelenghts in comparison to 0 h aging. Furthermore, for a given wavelenght, by comparing
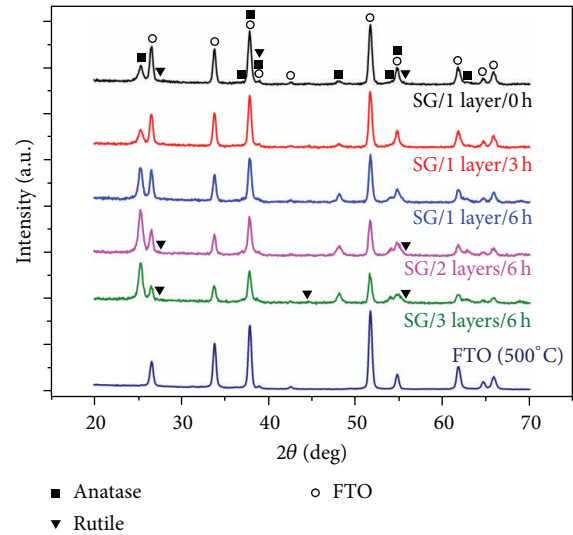

FIGURE 2: GA-XRD analysis of the different TiO_2 sol-gel photoelectrodes. The crystallinity of aged sol-gel is improved in comparison with the gel without aging (0 h). Anatase is the dominant phase in all the photoelectrodes, although a small amount of rutile is also present.
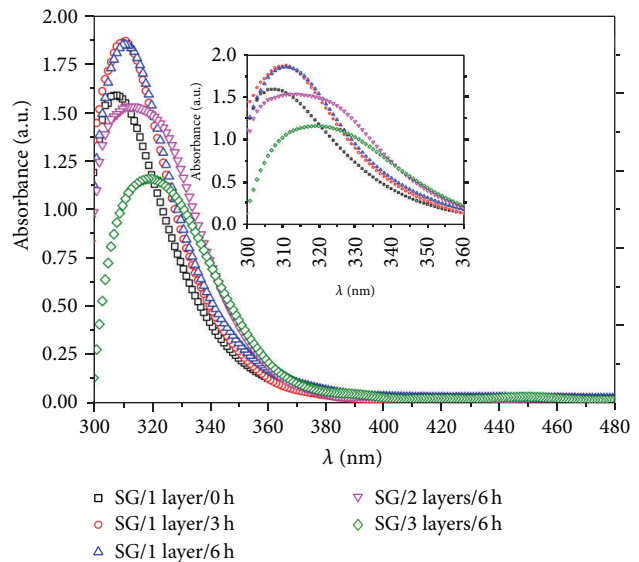

FIGURE 3: Absorbance (optical density) of the different sol-gel photoelectrodes. The slight changes in the optical properties induced by the aging time, as well as by the dip coating of multilayer photoelectrodes, are better appreciated in the inset.

the 1-layer photoelectrodes aged for difference times, it is evident that the absorbance intensity is higher in 6 h aged films. This is best appreciated in the region 300–320 nm, Figure 3, and must be a consequence of the chemical and physical changes [33] occuring within the sol. As previously discussed, the sizes of crystalline domains are very similar (approximately 30 nm) in all the photoelectrodes and cannot explain the differences in their optical properties. However, XRD analysis, Figure 2, has shown that aged photoelectrodes
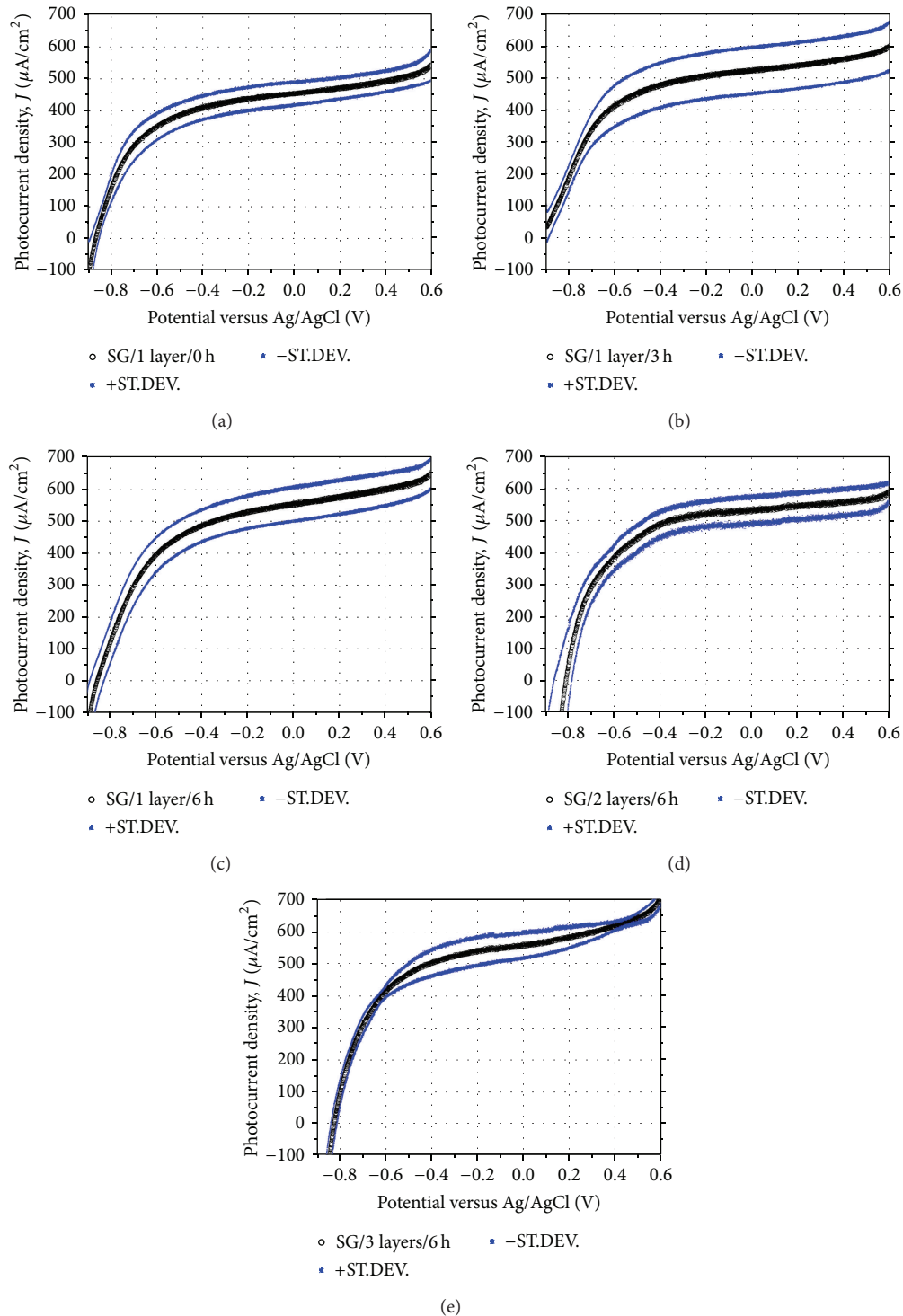
FIGURE 4: Effect of aging time on the photocurrent of TiO$_2$ sol-gel photoelectrodes: (a) SG/1 layer/0 h, (b) SG/1 layer/3 h, and (c) SG/1 layer/6 h. The effect of the thickness of TiO$_2$ on the photocurrent density is also reported; see (d) SG/2 layers/6 h and (e) SG/3 layers/6 h.

have a higher degree of crystallinity than nonaged films and, as a result, may interact differently with the incident light. We therefore tentatively assign the shift of the absorbance threshold to differences in the light scattering phenomena occuring within films aged for different times.

The optical properties are also in good agreement with the photocurrent measurements, reported in Figures 4(a)–4(c) for different aging times, 0, 3, and 6 h. By taking the value of the photocurrent density at 0.23 V versus Ag/AgCl (i.e., 1.23 V vs RHE in 1 M KOH), the reponse increases from

$460\,\mu A/cm^2$ for 0 h aging time to 550 and $570\,\mu A/cm^2$ in the case of 3 and 6 h aging time, respectively. The standard deviation between the photocurrent measurements for a given aging time is typically in the order of $\pm10\%$ and it can be concluded that there is no significant difference between the photoresponses of the sol-gel aged after 3 and 6 h, whereas the sol-gel with no aging (i.e., 0 h) clearly has the lowest performance. We ascribe the shift observed in the absorbance, Figure 3, and the enhanced photocurrent density in aged photoelectrodes, Figure 4, to the building-up of the sol-gel network occuring during the aging process. Clearly, the formation of such network has an impact on both the crystallinity and the optical properties as well as ability to collect the photogenerated electrons.

Additional information on the photoelectrochemical properties of sol-gel films is provided by the IPCE analysis in Figures 5(a)–5(c). The study of the IPCE curve, particularly in the region 300–340 nm, provides information on the electron transport properties of the photoelectrodes. What clearly emerges from the IPCE analysis, in good agreement with the photocurrent density measured previously discussed (Figures 4(a)–4(c)), is the superior ability of aged films (see comparison between 0 h aging, Figure 4(a), and 3 h, Figure 4(b), and 6 h aging, Figure 4(c)) to absorb photons and collect them at the back FTO electrode. Despite having practically the same IPCE in the range of 460 to 340 nm, the SG/1 layer/6 h photoelectrodes provide higher IPCE than SG/1 layer/0 h films for $\lambda < 340$ nm: 10% versus 7% at 340 nm, 17.5% versus 12.5% at 320 nm, and 26% versus 20% at 300 nm, as shown in Figures 5(a) and 5(c). The values for SG/1-layer/3 h aging, 7.5% at 340 nm, 14% at 320 nm, and 20% at 300 nm, Figure 5(b), are in between those of 0 and 6 h aging. The reason for the higher photocurrent density of 3 and 6 h aging times in comparison with 0 h aging time can therefore be confidently linked to the superior ability of aged photoelectrodes to collect electrons photogenerated from the absorption of shorter wavelength ($300\,nm \leq \lambda \leq 340\,nm$). Considering that the photoanodes were "front illuminated" and the absorption coefficient (α) of the light is a decreasing function of λ (i.e., shorter λ have higher α than longer λ), light of $300\,nm \leq \lambda \leq 340\,nm$ is mostly absorbed in the 10 to 100 nm region [34] closest to the electrolyte. Therefore, in the SG/1 layer/0–6 h aged photoelectrodes, the photogenerated electrons have to diffuse through the entire film ($0.6 \pm 0.1\,\mu m$) in order to be collected at the FTO back contact. This requires an excellent network interconnectivity, which can be ensured by aging the photoelectrodes, as clearly shown in Figures 4(a)–4(c) and Figures 5(a)–5(c). SEM analysis also reveals an additional feature responsible for the good performances of the SG photoelectrodes: their mesoporosity, Figures 6(a)-6(b), is in fact crucial to ensure penetration of the electrolyte within the photoanode. It should be noted that Figures 6(a)-6(b) show the microstructure of 6 h aged photoelectrodes; however, no significant differences in the morphology and mesoporosity of photoelectrodes aged for 0 or 3 h were observed. From the analysis of Figures 6(a)-6(b), it is not possible to provide an exact value for the pore size within the TiO_2 films; however, it is clear that such pores are bigger than 10 nm and are very likely to allow a good contact/interface

within the film and electrolyte [13]. In contrast, whenever the diameter of the pore is below 10 nm, the bulk of the film may not be in contact with the electrolyte and therefore does not contribute to the charge transfer process, limiting the film's photoactivity [23]. It is likely that the presence of 5wt.% PVB in the sol also contributes to establish such an optimal porous structure, although further studies are necessary to confirm this hypothesis.

The porosity of the thin films photoelectrodes has been estimated (from SEM micrograph) to be $21.8 \pm 0.6\%$, $20.2 \pm 0.7\%$, and $19.4 \pm 0.5\%$ for 0, 3, and 6 h aged photoelectrodes, respectively. As expected, considering the rather small window of investigated range of aging time (0 to 6 h), no major changes are observed. It has also been possible to estimate the specific surface area of the photoelectrodes by dye adsorption/desorption. Again, no significant differences were osberved, with values of $22 \pm 3\,m^2/g$, $20 \pm 2\,m^2/g$, and $19 \pm 2\,m^2/g$ for 0, 3, and 6 h aged photoelectrodes, respectively. Typically, larger modifications of surface area and porosity as a function of aging time are better appreciated by extending the aging to days or even weeks [35]. Nevertheless, there seems to be a trend suggesting a small decrease in porosity and surface area as the aging time increases; this could be due to further condensation reactions and formation of Ti–O–Ti within the sol. Such small changes of porosity and surface area (observed between 0 and 6 h aging time) may also contribute to generate differences in the light scattering behaviour and optical properties of the various photoelectrodes.

In addition to the influence of aging time, we have also investigated the effect of film thickness on the performances of the photoanodes, while keeping the aging time of the sol constant (6 h), attempting to optimize their light absorption properties. As it can be appreciated from Table 1, by increasing the number of dip-coated layers from 1 to 2 and 3, the thickness of the film increases from $0.6 \pm 0.1\,\mu m$ to $1.1 \pm 0.1\,\mu m$ and $1.6 \pm 0.2\,\mu m$, respectively. As an example, the SEM cross section profile of a SG/3-layer-thick photoanode is given in Figure 6(b).

The photocurrent measurements of multilayered photoanodes are reported in Figures 4(d)-4(e). By comparison with Figure 4(c) (1 layer, 6 h aging), it can be concluded that the photocurrent is not affected by the thickness/number of layers dip-coated on the FTO substrate and remains in the order of 550 to $570\,\mu A/cm^2$ at 0.23 V vs Ag/AgCl. Likewise, the IPCE curves of SG/2 layers/6 h and films, Figures 5(d)-5(e), are very similar to the IPCE response of SG/1 layer/6 h, Figure 5(c). The IPCE values of SG/3 layers/6 h, SG/2 layers/6 h, and SG/1 layer/6 h are, respectively, 12, 11, and 10% at 340 nm, 18, 19, and 17.5% at 320 nm, and 25, 25, and 26% at 300 nm. This is in contrast with a recent report [23] on a nearly linear increase in the IPCE on TiO_2 films up to $1.3\,\mu m$ thick, but once more it confirms the good electron transport properties of the photoelectrodes; the photogenerated charge carriers from light of $300\,nm \leq \lambda \leq 340\,nm$ can be also successfully collected in multilayers film (up to $1.6\,\mu m$ thick, Table 1).

Even at 300 nm, where the light's penetration depth is estimated to be 10–30 nm, based on the absorption spectrum
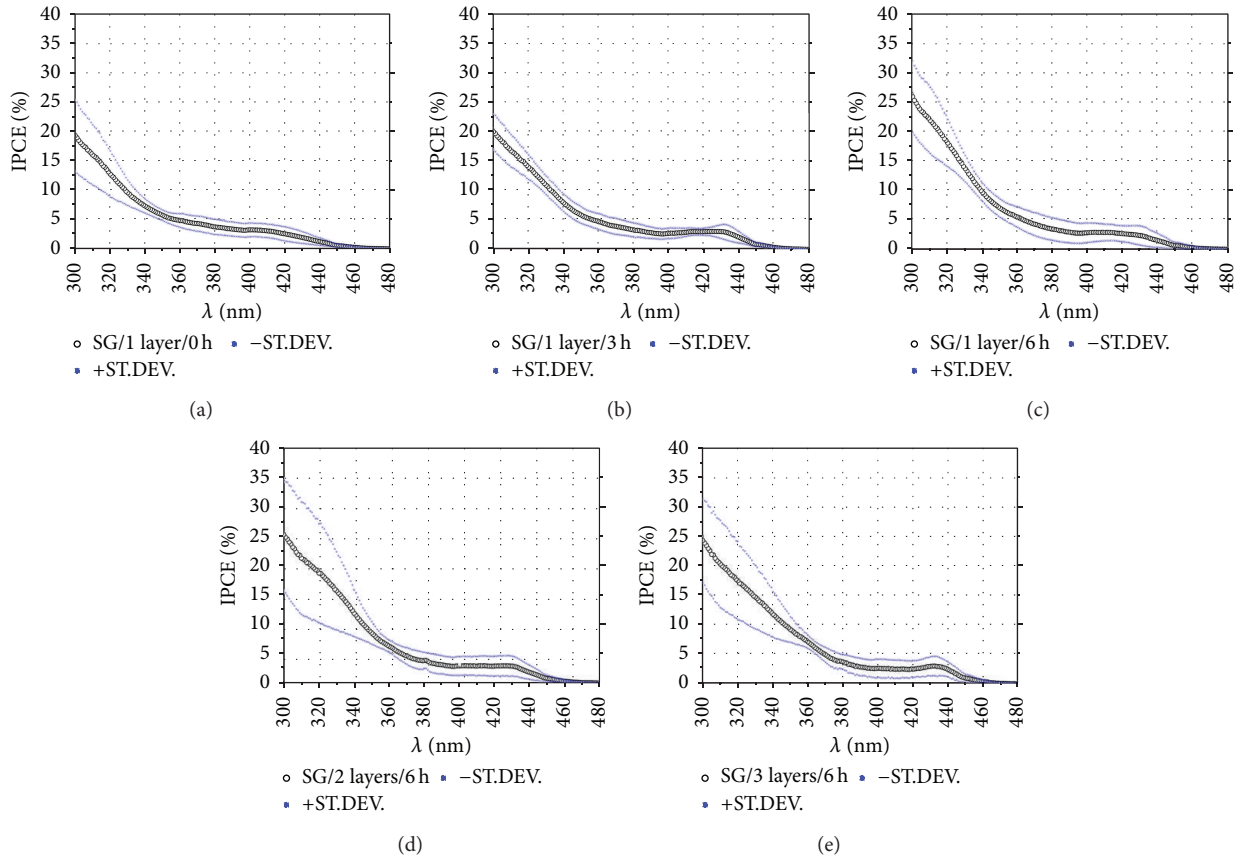
FIGURE 5: IPCE of the different types of sol-gel photoelectrodes investigated within this study: (a) SG/1 layer/0 h, (b) SG/1 layer/3 h, (c) SG/1 layer/6 h, (d) SG/2 layers/6 h, and (e) SG/3 layers/6 h.
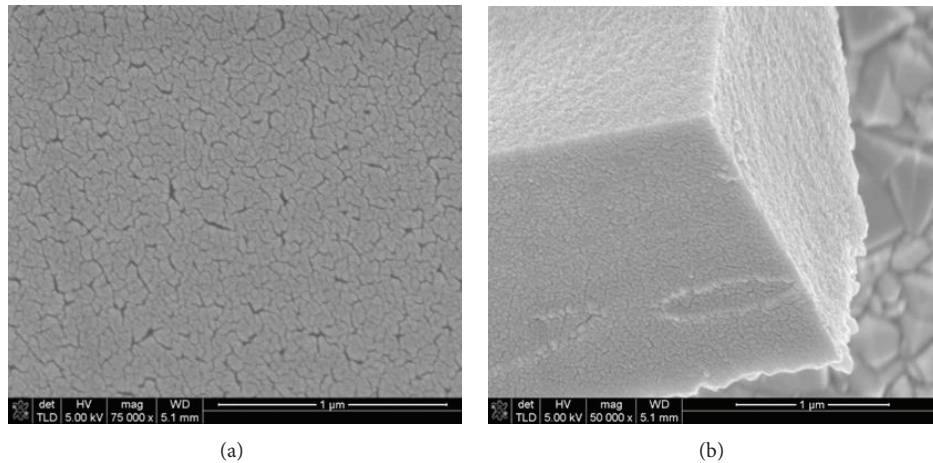

FIGURE 6: (a) Showing the mesoporosity of the SG photoelectrodes and (b) the view of a SG/3 layers/6 h photoelectrode. The mesoporosity of the film allows good penetration of the electrolyte within the film and it is likely to be responsible for the good photoactivity shown by the SG photoanodes.

by Eagles [34] and accounting for film's porosity and the presence of anatase [16], the IPCE is still 25% in both SG/3 layers/6 h and SG/2 layers/6 h. Films thinner than $0.6 \pm 0.1 \mu m$ (1 layer with dip coating parameter adopted within this work) were not considered in this study; it has

been recently reported that $0.2 \mu m$ thick mesoporous sol-gel provides photocurrent density (related to solar water splitting) in the range of $1 mA/cm^2$ [13] and it could be argued that also in our case thinner films may lead to an improved photoresponse. A final consideration to highlight
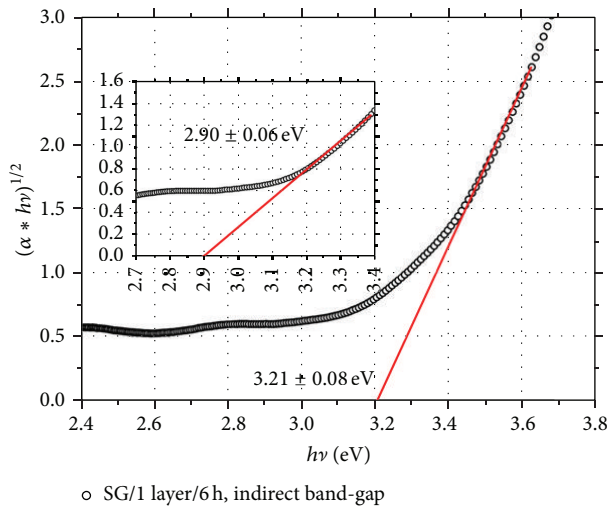
FIGURE 7: Tauc plot [25] of SG/1 layer/6 h photoelectrode. The indirect band-gap extrapolated from the plot is 3.21 ± 0.08 eV. An additional tail for a sub-band-gap of 2.9 ± 0.06 eV is also present. This indicates the presence of oxygen vacancies (shallow donors) within the photoanodes and explains the small IPCE signal observed for the photoelectrodes above 400 nm.

coating onto FTO substrates is crucial to ensure optimal performance of the photoelectrodes. It should be noticed that the aging time did not influence the thickness of the film. It is assumed that the concentration of the titanium tetraisopropoxide in the sol-gel system should instead affect the coating thickness (and should possibly also modify the long stability of the sol); this will be investigated in a separate study. The absorbance threshold of aged sol-gels is slightly shifted towards higher wavelenghts in comparison to 0 h aging and their photocurrent density (up to $570 \, \mu A/cm^2$, among the highest photocurrent densities reported for TiO_2 sol-gel) and IPCE response (10% at 340 nm and 26% at 300 nm) confirm the superiority of aged films also in terms of network interconnectivity and electron collection properties. It is also evident that the crystallinity of the films is improved after aging. No significant changes of the photoresponse were instead observed by increasing the thickness of the TiO_2 films. The presence of weak IPCE signals in all TiO_2 photoelectrodes, above 400 nm, is explained in terms of donor levels (oxygen vacancies) introduced during the processing and sintering of the sol-gel. Due to its wide band-gap (above 3 eV), TiO_2 alone cannot lead towards the development of photoelectrochemical water splitting devices with a 10% solar to hydrogen (STH) efficiency (the threshold above which such technology becomes industrially viable [27]). However, considering its unique properties, the study and the optimization of the photoelectrochemical behavior of TiO_2 based mesoporous photoanodes are very important, as we believe they can be used as an efficient, stable, and robust support for materials/particles capable of harvesting visible light.

Conflict of Interests

The authors declare that there is no conflict of interests regarding the publication of this paper.
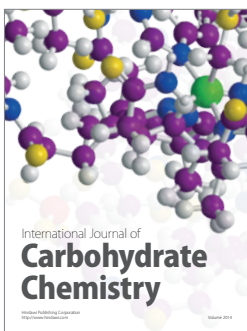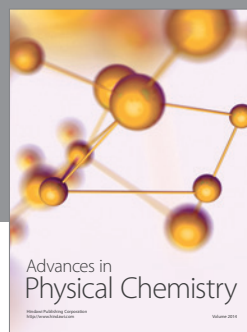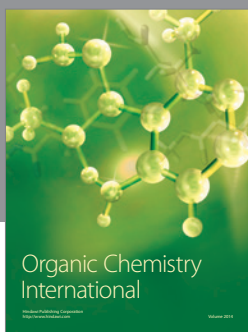
Acknowledgments

regarding the sol-gel photoelectrodes is their weak response in the region 400–440 nm, which can be appreciated in all the IPCE spectra, Figures 5(a)–5(e). The indirect band-gap of the photoelectrodes, Table 1, estimated by applying the Tauc plot to the optical data in Figure 3 is in the range of 3.21 to 3.25 eV, corresponding to an absorption threshold of 386.3 to 381.5 nm. The IPCE response well above the absorption threshold can be explained by the presence of shallow donor states within the TiO_2; for example, the use of carbon based precursors for the preparation of the TiO_2 sol-gel, as well as the sintering performed in air, is likely to introduce oxygen vacancies within the oxide. The presence of oxygen vacancies acting as donor states [36] also emerges from the Tauc plot of the photoelectrodes. As an example, the Tauc plot of SG/1 layer/6 h is shown in Figure 7. In addition to the indirect band-gap, extrapolated to be 3.21 ± 0.08 eV, there is a tail (Figure 7 inset) corresponding to a sub-band-gap of 2.90 ± 0.06 eV. Similar donor levels were also highlighted in a previous study on the activation energy for conduction in TiO_2 [37]. Finally, the trapping of a small amount of visible light within the photoanode could also be a consequence of the mesoporosity of the film, Figures 6(a)-6(b).

4. Conclusions

The optimization of a sol-gel process aimed at producing mesoporous TiO_2 based photoelectrodes for solar water splitting has been presented within this work. In particular, we have investigated two parameters, aging time of the sol and thickness of the TiO_2 films, and their impact on the photoelectrochemical properties of the material. Our results show that aging the sol for 3 to 6 h before the dip

References

[1] A. Fujishima and K. Honda, "Electrochemical photolysis of water at a semiconductor electrode," *Nature*, vol. 238, no. 5358, pp. 37–38, 1972.

[2] A. L. Linsebigler, G. Lu, and J. T. Yates Jr., "Photocatalysis on TiO$_2$ surfaces: principles, mechanisms, and selected results," *Chemical Reviews*, vol. 95, no. 3, pp. 735–758, 1995.

[3] T. Bak, J. Nowotny, M. Rekas, and C. C. Sorrell, "Photoelectrochemical hydrogen generation from water using solar energy. Materials-related aspects," *International Journal of Hydrogen Energy*, vol. 27, no. 10, pp. 991–1022, 2002.

[4] M. Ni, M. K. H. Leung, D. Y. C. Leung, and K. Sumathy, "A review and recent developments in photocatalytic water-splitting using TiO2 for hydrogen production," *Renewable and Sustainable Energy Reviews*, vol. 11, no. 3, pp. 401–425, 2007.

[5] A. Fujishima, X. Zhang, and D. A. Tryk, "TiO$_2$ photocatalysis and related surface phenomena," *Surface Science Reports*, vol. 63, no. 12, pp. 515–582, 2008.

[6] X. Chen and S. S. Mao, "Titanium dioxide nanomaterials: synthesis, properties, modifications and applications," *Chemical Reviews*, vol. 107, no. 7, pp. 2891–2959, 2007.

[7] J. A. Anta, "Electron transport in nanostructured metal-oxide semiconductors," *Current Opinion in Colloid and Interface Science*, vol. 17, no. 3, pp. 124–131, 2012.

[8] M. Radecka, A. Trenczek-Zajac, K. Zakrzewska, and M. Rekas, "Effect of oxygen nonstoichiometry on photo-electrochemical properties of TiO_{2-x}," *Journal of Power Sources*, vol. 173, no. 2, pp. 816–821, 2007.

[9] X. Chen, L. Liu, P. Y. Yu, and S. S. Mao, "Increasing solar absorption for photocatalysis with black hydrogenated titanium dioxide nanocrystals," *Science*, vol. 331, no. 6018, pp. 746–750, 2011.

[10] G. Wang, H. Wang, Y. Ling et al., "Hydrogen-treated TiO$_2$ nanowire arrays for photoelectrochemical water splitting," *Nano Letters*, vol. 11, no. 7, pp. 3026–3033, 2011.

[11] J. Augustynski and R. Solarska, "To what extent do the nanostructured photoelectrodes perform better than their macro-crystalline counterparts?" *Catalysis Science and Technology*, vol. 3, no. 7, pp. 1810–1814, 2013.

[12] E. Ghadiri, N. Taghavinia, S. M. Zakeeruddin, M. Grätzel, and J. Moser, "Enhanced electron collection efficiency in dye-sensitized solar cells based on nanostructured TiO2 hollow fibers," *Nano Letters*, vol. 10, no. 5, pp. 1632–1638, 2010.

[13] P. Hartmann, D. Lee, B. M. Smarsly, and J. Janek, "Mesoporous TiO$_2$: comparison of classical sol-gel and nanoparticle based photoelectrodes for the water splitting reaction," *ACS Nano*, vol. 4, no. 6, pp. 3147–3154, 2010.

[14] A. Hagfeldt and M. Grätzel, "Molecular photovoltaics," *Accounts of Chemical Research*, vol. 33, no. 5, pp. 269–277, 2000.

[15] J. Augustyński, B. D. Alexander, and R. Solarska, "Metal oxide photoanodes for water splitting," *Topics in Current Chemistry*, vol. 303, pp. 1–38, 2011.

[16] A. Wahl and J. Augustynski, "Charge carrier transport in nanostructured anatase TiO$_2$ films assisted by the self-doping of nanoparticles," *Journal of Physical Chemistry B*, vol. 102, no. 40, pp. 7820–7828, 1998.

[17] D. Regonini, A. C. Teloeken, A. K. Alves et al., "Electrospun TiO$_2$ fiber composite photoelectrodes for water splitting," *ACS Applied Materials & Interfaces*, vol. 5, no. 22, pp. 11747–11755, 2013.

[18] E. Stathatos, P. Lianos, and C. Tsakiroglou, "Highly efficient nanocrystalline titania films made from organic/inorganic nanocomposite gels," *Microporous and Mesoporous Materials*, vol. 75, no. 3, pp. 255–260, 2004.

[19] Y. Chen, E. Stathatos, and D. D. Dionysiou, "Microstructure characterization and photocatalytic activity of mesoporous TiO$_2$ films with ultrafine anatase nanocrystallites," *Surface and Coatings Technology*, vol. 202, no. 10, pp. 1944–1950, 2008.

[20] D. Hidalgo, R. Messina, A. Sacco et al., "Thick mesoporous TiO$_2$ films through a sol-gel method involving a non-ionic surfactant: characterization and enhanced performance for water photoelectrolysis," *International Journal of Hydrogen Energy*, 2014.

[21] A. Yasumori, K. Ishizu, S. Hayashi, and K. Okada, "Preparation of a TiO2 based multiple layer thin film photocatalyst," *Journal of Materials Chemistry*, vol. 8, no. 11, pp. 2521–2524, 1998.

[22] A. Yasumori, H. Shinoda, Y. Kameshima, S. Hayashi, and K. Okada, "Photocatalytic and photoelectrochemical properties of TiO$_2$-based multiple layer thin film prepared by sol-gel and reactive-sputtering methods," *Journal of Materials Chemistry*, vol. 11, no. 4, pp. 1253–1257, 2001.

[23] J. Krýsa, M. Baudys, M. Zlámal, H. Krýsová, M. Morozová, and P. Klusoň, "Photocatalytic and photoelectrochemical properties of sol-gel TiO$_2$ films of controlled thickness and porosity," *Catalysis Today*, vol. 230, pp. 2–7, 2014.

[24] A. K. Alves, F. A. Berutti, F. J. Clemens, T. Graule, and C. P. Bergmann, "Photocatalytic activity of titania fibers obtained by electrospinning," *Materials Research Bulletin*, vol. 44, no. 2, pp. 312–317, 2009.

[25] J. Tauc, "Absorption edge and internal electric fields in amorphous semiconductors," *Materials Research Bulletin*, vol. 5, no. 8, pp. 721–729, 1970.

[26] A. Fattori, *Electrochemical and Spectroelectrochemical studies of dyes used in dye-sensitized solar cells [Ph.D. thesis]*, University of Bath, 2010.

[27] R. van de Krol and M. Gratzel, *Photoelectrochemical Hydrogen Production*, Springer, New York, NY, USA, 2012.

[28] L. L. Hench and J. K. West, "The Sol-Gel process," *Chemical Reviews*, vol. 90, no. 1, pp. 33–72, 1990.

[29] C. J. Brinker and G. W. Scherer, *Sol-gel Science: The Physics and Chemistry of Sol-gel Processing*, Academic Press, San Diego, Calif, USA, 1990.

[30] V. G. Kessler, G. I. Spijksma, G. A. Seisenbaeva, S. Håkansson, D. H. A. Blank, and H. J. M. Bouwmeester, "New insight in the role of modifying ligands in the sol-gel processing of metal alkoxide precursors: a possibility to approach new classes of materials," *Journal of Sol-Gel Science and Technology*, vol. 40, no. 2-3, pp. 163–179, 2006.

[31] T. Sreethawong, Y. Suzuki, and S. Yoshikawa, "Synthesis, characterization, and photocatalytic activity for hydrogen evolution of nanocrystalline mesoporous titania prepared by surfactant-assisted templating sol-gel process," *Journal of Solid State Chemistry*, vol. 178, no. 1, pp. 329–338, 2005.

[32] A. L. Patterson, "The scherrer formula for X-ray particle size determination," *Physical Review*, vol. 56, no. 10, pp. 978–982, 1939.

[33] H. Sakamoto, J. Qiu, and A. Makishima, "The preparation and properties of CeO$_2$-TiO$_2$ film by sol-gel spin-coating process," *Science and Technology of Advanced Materials*, vol. 4, no. 1, pp. 69–76, 2003.

[34] D. M. Eagles, "Polar modes of lattice vibration and polaron coupling constants in rutile (TiO$_2$)," *Journal of Physics and Chemistry of Solids*, vol. 25, no. 11, pp. 1243–1251, 1964.

[35] C. J. Brinker, R. Sehgal, S. L. Hietala et al., "Sol-gel strategies for controlled porosity inorganic materials," *Journal of Membrane Science*, vol. 94, pp. 85–102, 1994.

[36] A. Janotti, J. B. Varley, P. Rinke, N. Umezawa, G. Kresse, and C. G. van de Walle, "Hybrid functional studies of the oxygen vacancy in TiO$_2$," *Physical Review B—Condensed Matter and Materials Physics*, vol. 81, no. 8, Article ID 085212, 7 pages, 2010.

[37] D. Regonini, V. Adamaki, C. R. Bowen, S. R. Pennock, J. Taylor, and A. C. E. Dent, "AC electrical properties of TiO$_2$ and Magnéli phases, TinO$_{2n-1}$," *Solid State Ionics*, vol. 229, pp. 38–44, 2012.

International Journal of
Medicinal Chemistry

Organic Chemistry
International

International Journal of
Photoenergy

International Journal of
Analytical Chemistry

Advances in
Physical Chemistry

International Journal of
Carbohydrate
Chemistry

Journal of
Quantum Chemistry

The Scientific
World Journal
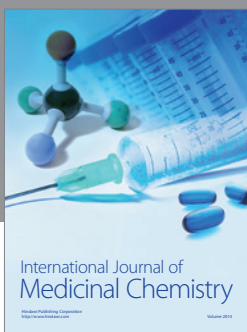
Submit your manuscripts at
http://www.hindawi.com

Hindawi

Journal of
Analytical Methods
in Chemistry

Journal of
Spectroscopy

International Journal of
Inorganic Chemistry

International Journal of
Electrochemistry

Journal of
Applied Chemistry

Bioinorganic Chemistry
and Applications

Journal of
Theoretical Chemistry

Chromatography
Research International

Journal of
Catalysts

Journal of
Chemistry

International Journal of
Spectroscopy